

# Cluster Dynamics Modeling of Niobium and Titanium Carbide Precipitates

Nadezda Korepanova<sup>a,b,\*</sup>, Mihai Dima<sup>c</sup>, Long Gu<sup>a,b,d,e,\*</sup>, Hushan Xu<sup>a,b</sup>

<sup>a</sup>*Institute of Modern Physics, Chinese Academy of Sciences, Lanzhou, China*

<sup>b</sup>*School of Nuclear Science and Technology, University of Chinese Academy of Sciences, Beijing, China*

<sup>c</sup>*Institute for Physics and Nuclear Engineering, Str. Atomistilor 407, P.O. Box MG-6, R-76900 Bucharest, Romania*

<sup>d</sup>*School of Nuclear Science and Technology, Lanzhou University, Lanzhou 730000, China*

<sup>e</sup>*Paul Scherrer Institute, Villigen, Switzerland*

---

## Abstract

Kinetics of niobium and titanium carbide precipitates in iron has been simulated with cluster dynamics. The simulations, carried out in austenite and ferrite for niobium carbides, respectively in austenite for titanium carbide, were analyzed for dependency on temperature, solute concentration and initial cluster distribution. The results are presented for different temperatures and solute concentrations and compared to available experimental data. They show little impact of initial cluster distribution beyond a certain relaxation time and that highly dilute alloys with only monomers present a significantly different behavior than less dilute alloys or alloys with different initial cluster distribution.

**Keywords:** cluster dynamics, precipitates, precipitation kinetics, titanium carbide, niobium carbide

---

## 1. Introduction

Addition of titanium and niobium to steels in metallurgy is conducive to titanium/niobium carbide precipitates in solid solution due to their combination with the carbon present in the steel. This process limits the formation of chromium carbides, thereby preventing intergranular corrosion [1, 2]. Additionally, finely dispersed carbide precipitates increase alloy strengths both at low and high temperature [2, 3]. Nuclear-grade steels are required to meet higher, additional standards, and the question of precipitate dynamics is raised with respect to them acting as point defect recombination centers and sinks for helium, which reduces void swelling and helium embrittlement [4, 5, 6, 7, 8]. TiC/NbC precipitates tend to stabilize dislocation networks, and hence enhance creep resistance [9, 10]. Titanium carbides are in particular attractive in this respect, which led to the development of 15-15Ti steel in the 1970's [11] for nuclear reactor applications. This steel exhibits

excellent resistance to irradiation swelling and creep and has been chosen as structural material for several Generation-IV designs.

To simulate the precipitation behavior of carbides we used cluster dynamics (CD), which is an effective method to predict microstructural evolution in a material - with little computing overhead for long time period simulations. In this method polyatomic clusters embedded in the solid solution exchange solute atoms by absorption or emission. Time evolution of cluster distributions is computed from differential equations coupled through monomer exchanges.

In the case of iron CD has yielded good results for Cu precipitates in ferrite [12] and MnSiNi precipitates in ferrite-martensitic steel [14].

For NbC and TiC precipitates in steel classical kinetic nucleation theory (CNT) has been used [15, 22, 16, 17], TiC precipitate modelling focusing more on Precipitation-Temperature-Time (PTT) diagrams, rather than on time-evolution of mean radius, volume fraction, and number density.

This paper is organized as follows: Section 2 gives a brief description of the CD method; Section 3 presents our simulation results for niobium carbides in austenite and ferrite and for titanium carbide in austenite; Section 3 presents a comparison of our

---

\*Corresponding authors at: Institute of Modern Physics, Chinese Academy of Sciences, Lanzhou, China.

E-mail addresses: nadezhda\_kv@bk.ru (N. Korepanova), gulong@impcas.ac.cn (L. Gu).

results to existing experimental data; and Section 4 summarises our study.

## 2. Methodology

In cluster dynamics alloys are treated as binary systems of an alloy matrix with clusters of solute atoms. Clusters grow or shrink through the absorption, respectively emission of solute atoms. Time evolution of solute clusters is dictated by a set of differential equations (1-2) which assume only monomers to be mobile. Small cluster mobility may result from common drift of monomers, an assumption reasonable in dilute alloys [18].

$$\frac{dC_n}{dt} = \beta_{n-1}C_1C_{n-1} - (\alpha_n + \beta_nC_1)C_n + \alpha_{n+1}C_{n+1}, \quad n \neq 1, \quad (1)$$

$$\frac{dC_1}{dt} = -2\beta_1C_1C_1 + \alpha_2C_2 + \sum_{i=2}^{N_{max}} [\alpha_i - \beta_iC_1]C_i, \quad (2)$$

where  $n$  is the cluster size,  $N_{max}$  the maximal cluster size,  $C_n$  the uniform concentration of size  $n$  clusters,  $C_1$  the concentration of monomers,  $\alpha_n$  the rate of monomer emission from size  $n$  clusters,  $\beta_n$  the rate of monomer absorption by size  $n$  clusters, the latter two calculated as:

$$\beta_n = 4\pi r_n D / V_{at}^m, \quad (3)$$

$$\alpha_n = \beta_{n-1}C_{eq}^{sol} \exp \left[ \frac{A [\sigma n^{2/3} - \sigma(n-1)^{2/3}]}{kT} \right], \quad (4)$$

where  $V_{at}^m$  is the atomic volume of the alloy-matrix,  $r_n$  the radius of size  $n$  clusters,  $D$  the thermal diffusion coefficient of solute atoms in the system,  $A$  the geometrical factor,  $\sigma$  the interfacial energy between precipitates and matrix,  $C_{eq}^{sol}$  the equilibrium concentration of solute atoms in the system,  $T$  the temperature in degrees Kelvin, and  $k$  the Boltzmann constant. The radius of size  $n$  clusters is:

$$r_n = \left( \frac{3nV_{at}^p}{4\pi} \right)^{1/3}. \quad (5)$$

CD is a computationally efficient method, however with increasing  $N_{max} \gtrsim 100$  it can become CPU wise prohibitive. A traditional way to overcome this is to transform the differential equations into a Fokker-Planck partial differential equation [19, 20]:

$$\frac{\partial C_n}{\partial t} = -\frac{\partial}{\partial n} [(\beta_nC_1 - \alpha_n)C_n] + \frac{1}{2} \frac{\partial^2}{\partial n^2} [(\beta_nC_1 + \alpha_n)C_n], \quad (6)$$

The discretization of the Fokker-Planck equation using the central difference method brings Eq.6 into the following form:

$$\begin{aligned} \frac{dC_{n_j}}{dt} = & \frac{C_{n_{j-1}}}{n_{j+1} - n_{j-1}} \times \\ & \times \left[ (\beta_{n_{j-1}}C_1 - \alpha_{n_{j-1}}) + \frac{\beta_{n_{j-1}}C_1 + \alpha_{n_{j-1}}}{n_j - n_{j-1}} \right] - \\ & - \frac{C_{n_j}}{n_{j+1} - n_{j-1}} (\beta_{n_j}C_1 + \alpha_{n_j}) \times \\ & \times \left[ \frac{1}{n_{j+1} - n_j} + \frac{1}{n_j - n_{j-1}} \right] + \\ & + \frac{C_{n_{j+1}}}{n_{j+1} - n_{j-1}} \times \\ & \times \left[ -(\beta_{n_{j+1}}C_1 - \alpha_{n_{j+1}}) + \frac{\beta_{n_{j+1}}C_1 + \alpha_{n_{j+1}}}{n_{j+1} - n_j} \right], \end{aligned} \quad (7)$$

and the evolution of monomer concentration to:

$$\begin{aligned} \frac{dC_1}{dt} = & -2\beta_1C_1C_1 + \alpha_2C_2 + \sum_{j=2}^{N_{tr}} [\alpha_j - \beta_jC_1]C_j + \\ & + \sum_{j>N_{tr}}^{N_{max}} [\alpha_j - \beta_jC_1]C_j \frac{n_{j+1} - n_{j-1}}{2}. \end{aligned} \quad (8)$$

where  $n_j$  is defined as follows:

$$\begin{cases} n_j = j, \forall j \leq N_{tr}, \\ n_j = N_{tr} + \frac{1-\lambda^j - N_{tr}}{1-\lambda}, \forall j > N_{tr}, \end{cases} \quad (9)$$

The above system is reduced to the initial differential equations for  $n_j = j$ . This numerical scheme does not strictly conserve matter (as do differential equations (1) and (2)), however under carefully defined circumstances the losses are small and acceptable. To solve the above system we used in our study the ODEINT solver [21].

In this study we assume the diffusion coefficient of titanium/niobium carbide to be determined by the most resistive element, i.e. - we used the Ti and Nb diffusion coefficients in the simulation, correspondingly.

References [34] and [16] cite the “pipe-diffusion” effect for TiC/NbC precipitation kinetics, respectively a faster solute diffusion along dislocations than in the lattice in general. We included the effect of dislocations in the model, in Eq.3, as a modified effective diffusivity [16]:

$$D_{eff} = D_{disl}\pi R_{core}^2\rho + D_{bulk}(1 - \pi R_{core}^2\rho), \quad (10)$$

where  $D_{disl}$  is the diffusion along dislocations (equal to  $D_{bulk}\alpha_{disl}$ , with  $\alpha_{disl}$  a correction factor defined according to [23] and presented in Table 2),  $D_{bulk}$  the bulk diffusivity,  $R_{core}$  the radius of the dislocation core, and  $\rho$  the dislocation density. Fig. 1 illustrates the effect of dislocations on diffusivity and how this changes with temperature. The figure shows the ratio of effective diffusivity to bulk diffusivity in austenite steel for several values of dislocation densities. The ratio increases with dislocation density increase and drops sharply with increasing temperature.

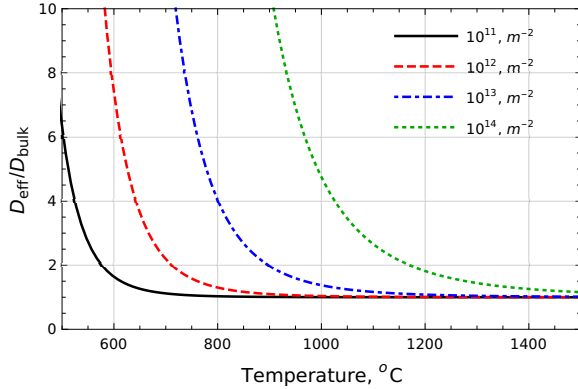


Figure 1: Effect of dislocation on diffusivity - the ratio of effective diffusivity to bulk diffusivity in austenite steel for several values of dislocation densities.

The results of the simulation are the time-evolution of the mean radius, the  $\bar{r}$  volume fraction,  $f_v$ , and the number density of precipitates,  $N_{tot}$  - calculated with the following equations:

- Mean radius

$$\bar{r} = \left( \frac{3\bar{n}V_{at}^p}{4\pi} \right)^{1/3}, \quad (11)$$

where  $V_{at}^p$  is the atomic volume of precipitate, and  $\bar{n}$  the mean size of precipitate clusters:

$$\bar{n} = \frac{\sum_{j_{cut}}^{N_{max}} n_j C_{n_j} \Delta n_j}{\sum_{j_{cut}}^{N_{max}} C_{n_j} \Delta n_j}, \quad (12)$$

with  $\Delta n_j = n_j - n_{j-1}$ ,  $j_{cut}$  taken such that  $r_{j_{cut}} = 1 \text{ nm}$  for TEM data (given the resolution limit in [24, 25], and  $r_{j_{cut}} = 0.5 \text{ nm}$  for SANS data).

- Volume fraction

$$f_v = \frac{V_{at}^p}{V_{at}^{mat}} \sum_{j_{cut}}^{N_{max}} n_j C_{n_j} \Delta n_j \times 100\%. \quad (13)$$

- Number density

$$N_{tot}(t) = \frac{1}{V_{at}^{mat}} \sum_{j_{cut}}^{N_{max}} C_{n_j}(t) \Delta n_j, \quad (14)$$

with  $V_{at}^{mat}$  the atomic volume of the matrix.

In our study we used an initial cluster distribution described by:

$$\begin{cases} C_1 = xC_0, \\ C_n = \frac{(100-x)C_0}{n \sum_{n=1}^M \Delta n}, & 2 \leq n \leq M \\ C_n = 0, & n > M \end{cases} \quad (15)$$

where  $C_0$  is the concentration of the alloying element in steel,  $x$  the part of the alloying element in monomer form,  $M$  the maximal cluster size assumed to exist in the steel at moment  $t = 0$ . In the next section, we show the dependence of CD results on the initial state of the system.

### 3. Results and Discussion

In this section, we present the results of our CD simulations for NbC and TiC in ferrite and austenite and compare them with experimental data from literature. The parameters used in the simulations are shown in Tables 1 and 2. Table 1 displays the material parameters for TiC, NbC and iron matrix and Table 2 gives references to experimental data and the conditions under which they was obtained.

Table 1: Material parameters for Titanium and Niobium carbides and for the Iron matrix.

	Parameter	Symbol	Units	Value	Reference
TiC	Lattice parameter	$a$	$nm$	0.433	[26]
	$\gamma Fe$				
	Diffusion coefficient	$D^{Ti}$	$m^2/s$	$0.15 \cdot 10^{-4} \exp[-251000/RT]$	[27]
	Interfacial energy	$\sigma$	$J/m^2$	0.2	[28]
NbC	solubility limit	$\log[MC]$		$2.97 - 6780/T$	[29]
	Lattice parameter	$a$	$nm$	0.445	[30]
	$\gamma Fe$				
	Diffusion coefficient	$D^{Nb}$	$m^2/s$	$0.75 \cdot 10^{-4} \exp[-264000/RT]$	[31]
$\alpha Fe$	Interfacial energy	$\sigma$	$J/m^2$	$1.0058 - 0.4493 \cdot 10^{-3} T(K^\circ)$	[32]
	solubility limit	$\log[MC]$		$2.06 - 6770/T$	
	Diffusion coefficient	$D^{Nb}$	$m^2/s$	$1.27 \cdot 10^{-5} \exp[-224000/RT]$	[17]
	Interfacial energy	$\sigma$	$J/m^2$	0.5	[17]
Matrix	solubility limit	$\log[MC]$		$5.43 - 10960/T$	[17]
	Lattice parameter	$a_{\gamma Fe}$	$nm$	0.358	
	Lattice parameter	$a_{\alpha Fe}$	$nm$	0.287	
	Correction factort	$\alpha_{disl}(\gamma Fe)$		$0.643 \exp(118700/(R * T))$	[23]
	Correction factor	$\alpha_{disl}(\alpha Fe)$		$0.0133 \exp(115000/(R * T))$	[23]

Table 2: Experimental datasets and the concentrations and temperatures at which they were measured.

Reference	Ti/Nb, wt%	C, wt%	Temperatures, $^{\circ}C$	Matrix	Dislocation density, $m^{-2}$
TiC					
[25]	0.31	0.1	T=750	$\gamma Fe$	$6 \cdot 10^{14}$ (from [25])
[33, 34]	0.1	0.05	T=925	$\gamma Fe$	$3.24 \cdot 10^{13}$ (calc. from [34])
[28]	0.4	0.07	T=900	$\gamma Fe$	– (assumed $6 \cdot 10^{14}$ )
[36]	0.25	0.05	T=900	$\gamma Fe$	– (assumed $6 \cdot 10^{14}$ )
NbC					
[24]	0.031/0.095	0.1/0.1	T=900/950	$\gamma Fe$	– (assumed $10^{11}$ )
[35, 17]	0.040/0.079	0.0058/0.01	T=600/700/800	$\alpha Fe$	$2 \cdot 10^{14}$ (from [35, 17])

### 3.1. Niobium Carbide

Figures 2 and 3 show the dependence on the initial cluster distribution for the time-evolution of precipitate mean radius and number density. We assessed this in order to check the sensitivity of our simulations to the initial state of the system. The initial cluster distributions for our simulations are described by Eq.15. Note in the figures that we index the radius  $r_M$  by  $M$ , the maximal size of a cluster initially existing in the system. The cluster distributions we used were both described by Eq.15, as well as arbitrary distributions: Poisson-like, or step-function. The simulation results are however the same for all distributions, warranting our use of Eq.15 described initial distributions throughout our study.

Figure 2 shows the time-evolution of precipitate mean radius and number density in 4 distinct cases for which we varied the concentrations of monomers and other clusters (see Eq.15), while keeping  $r_M$  constant. Complementary, Figure 3

presents the time-evolution of the mean radius and number density in relation to  $r_M$ , for the same corresponding monomer concentrations. As comparison Figure 3 shows the simulation only for monomers.

As evident in Figures 2 – 3 the initial cluster distributions play a role only in the initial departure time (with the notable exception of the 0.031wt%Nb-steel simulation, with monomers and very small clusters). After 1000 s the effect of the initial cluster distribution washes out and all simulations become indistinguishable from one another. The exception case of 0.031wt%Nb-steel with monomers and very small clusters is shown in Fig.3. Its anomalous behaviour was also observed for TiC in  $\gamma Fe$  and NbC in  $\alpha Fe$ . A possible explanation could be that in dilute alloys there are few precipitation centers, which have the opportunity to grow faster than in the case of higher solute concentrations. The amount of such clusters remains however small (see upper Fig.3). Had we

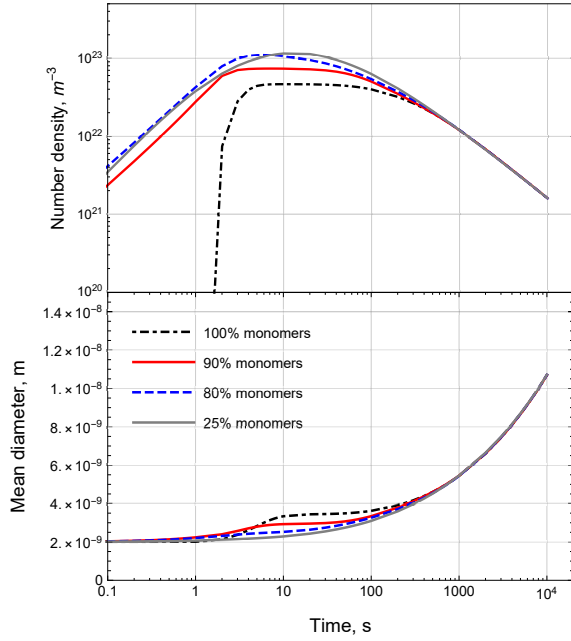


Figure 2: Dependence of simulation results on initial cluster distributions.  $T=950^{\circ}\text{C}$ ,  $C(\text{wt}\%\text{Nb})=0.095$ .

introduced higher clusters in the initial distribution, the precipitate kinetic would have followed the standard behaviour.

Comparing our simulations (Fig.4) with experimental data for niobium carbide precipitates in austenite [24] we find that in 0.031wt%Nb-steel 90% of niobium should exist as monomers - because if we would accept the 100% assertion of [24], the simulations would contradict the experimental data. We assume<sup>1</sup> that the remaining 10% are distributed in clusters with  $r_M < 1\text{nm}$  is invisible to TEM.

For niobium carbide precipitates in ferrite the simulation results and experimental data [17, 35] are depicted in Fig.5. Our model with the set of parameters from Table 1 matches quite well the experimental data of [17, 35], less to some extent the volume fraction, predicting faster clustering of the precipitates than experimentally observed. Fig.5 also shows better agreement with experimental data at low temperatures versus high

<sup>1</sup>The exact dislocation density for the steel used by Hansen et al. [24] is not available. Hence, we adjusted this parameter to agree with the experimental data. The result shows the dislocation density of steel to be in the range  $10^{11} - 10^{12} \text{ m}^{-2}$ . This concurs with the mention that the steel was well annealed [24].

temperatures. This could be due to the higher energy available at high temperature that activates the diffusion of small clusters along with monomers, whereas in our model only the monomers are mobile.

### 3.2. Titanium Carbide

Simulation results for TiC precipitates in austenite and experimental data from [25, 28, 33, 36] are presented in Figures 6 – 8. Fig.6 displays the time evolution of mean particle diameter - CD predicting a particle diameter  $\propto t^{1/3}$ , regardless concentration, temperature, and dislocation density (except in 0.1wt%Ti-steel  $\propto t^{1/2}$ ). Experimental data on the other hand exhibits two regions: an initial region, with mean diameter is proportional to time exponent with factor 0.5-1.0; and a secondary region with the time exponent having a very low factor, practically a plateau. Although in [36] the secondary region is considered  $\propto t^{1/3}$  (reflecting the Ostwald ripening phenomenon controlled by bulk diffusion of Ti), the authors believe the time exponent has a much lower factor (likely due to a different phenomenon). The two regions are also clearly observed in the size distributions.

The size distributions from experimental data [36] are shown in Fig.7. Although our model predicts a smaller mean diameter, the overall distribution shape of the sizes is strikingly similar to experimental one (up to 3610 s, after which the distributions start to differ). Additionally, in the inserts in Fig. 7 the experimental and simulated size distributions are plotted such that both have the same mean diameter and maximal magnitude. The comparison of size distributions relative to the experiment [25] at  $750^{\circ}\text{C}$  (Fig.8) shows a similar change in size distribution. The small difference observed might suggest a competing mechanism controlling the growth of TiC precipitates.

In [25] it was mentioned that the pinning of mobile dislocation affects TiC precipitate kinetics in the temperature range  $650 - 900^{\circ}\text{C}$ . However, CD applies only diffusion-controlled growth of precipitate clusters. To overcome this obstacle, a model for time-evolution of mobile dislocation density should be introduced alongside with the dependency of diffusion on mobile dislocation density. The verification of this suggestion is postponed to further study. Note that the data itself is very scarce for TiC precipitations. We assess that there is a necessity

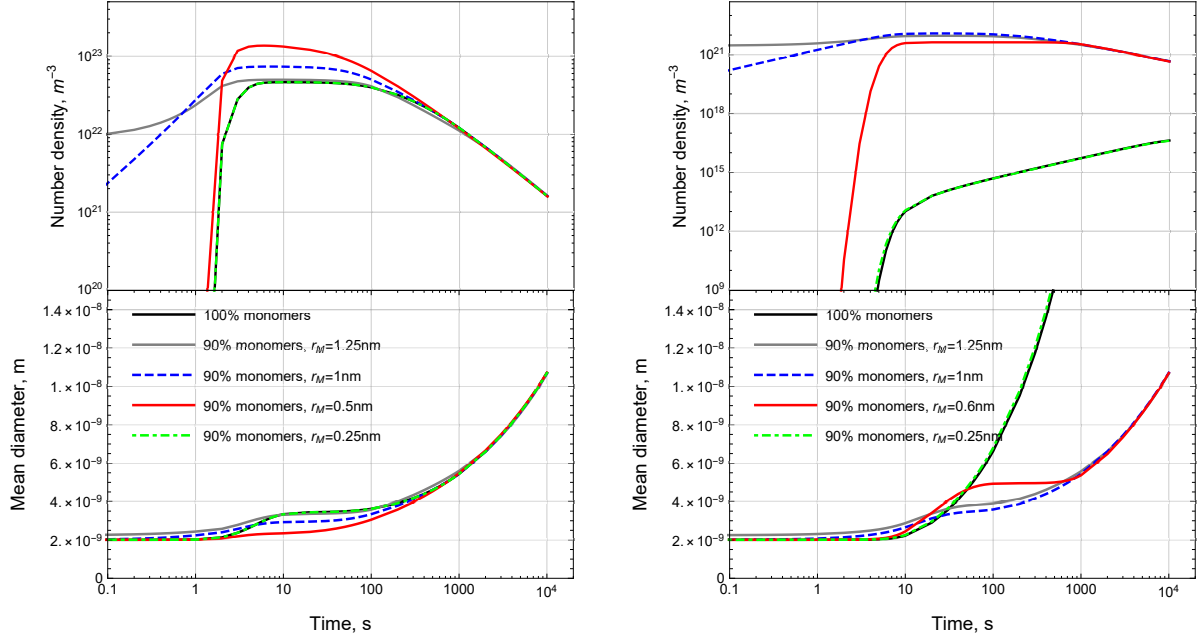


Figure 3: Dependence of simulation results on initial cluster distributions and radius  $r_M$ .  $T=950^\circ\text{C}$ ,  $C(\text{wt\%Nb})=0.095$  (left graph),  $C(\text{wt\%Nb})=0.031$  (right graph).

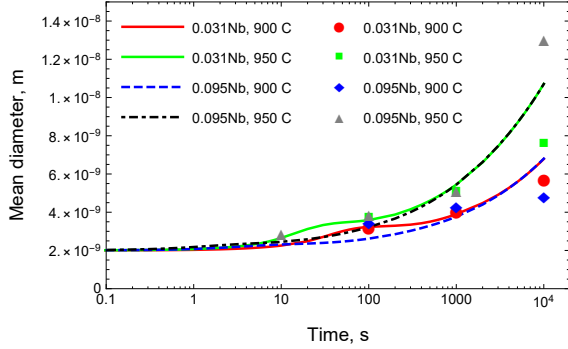


Figure 4: Comparison of simulation results with experimental data for NbC precipitates in austenitic stainless steel. The dots represent the experimental data of [24].

for more experimental and theoretical work on TiC precipitates.

#### 4. Conclusion

In the present paper we applied cluster dynamics to model precipitation kinetics of niobium and titanium carbides in steels. The kinetic of NbC precipitates have been simulated for ferritic and austenitic iron matrices. Our simulation results are in agreement with experimental data. We have analyzed the results for dependency on initial

cluster distribution, where we considered various types of distributions and monomers concentration. The analysis has shown that the initial distribution plays a role only in the initial-time range. After an initial-time all simulations follow the same pattern. The analysis has also shown the “special” behavior of precipitates if only monomers are present in very dilute alloys: the fast growth of mean particle diameter, while number density remains small. We have suggested that in dilute alloy fewer precipitation centers are created and they have less competition, which allows those centers to grow faster.

For TiC on the other hand, the simulation results and experimental data differ more pronounced. This could be explained by another controlling mechanism besides diffusion. Such mechanism could be mobile dislocation and its pinning, which was suggested in [25]. We believe, that more experimental and theoretical work is needed to correctly model titanium carbide precipitates kinetics.

#### Acknowledgments

N. Korepanova is grateful for the CAS-TWAS President’s Fellowship Programme for this doctoral fellowship (2016CTF004).

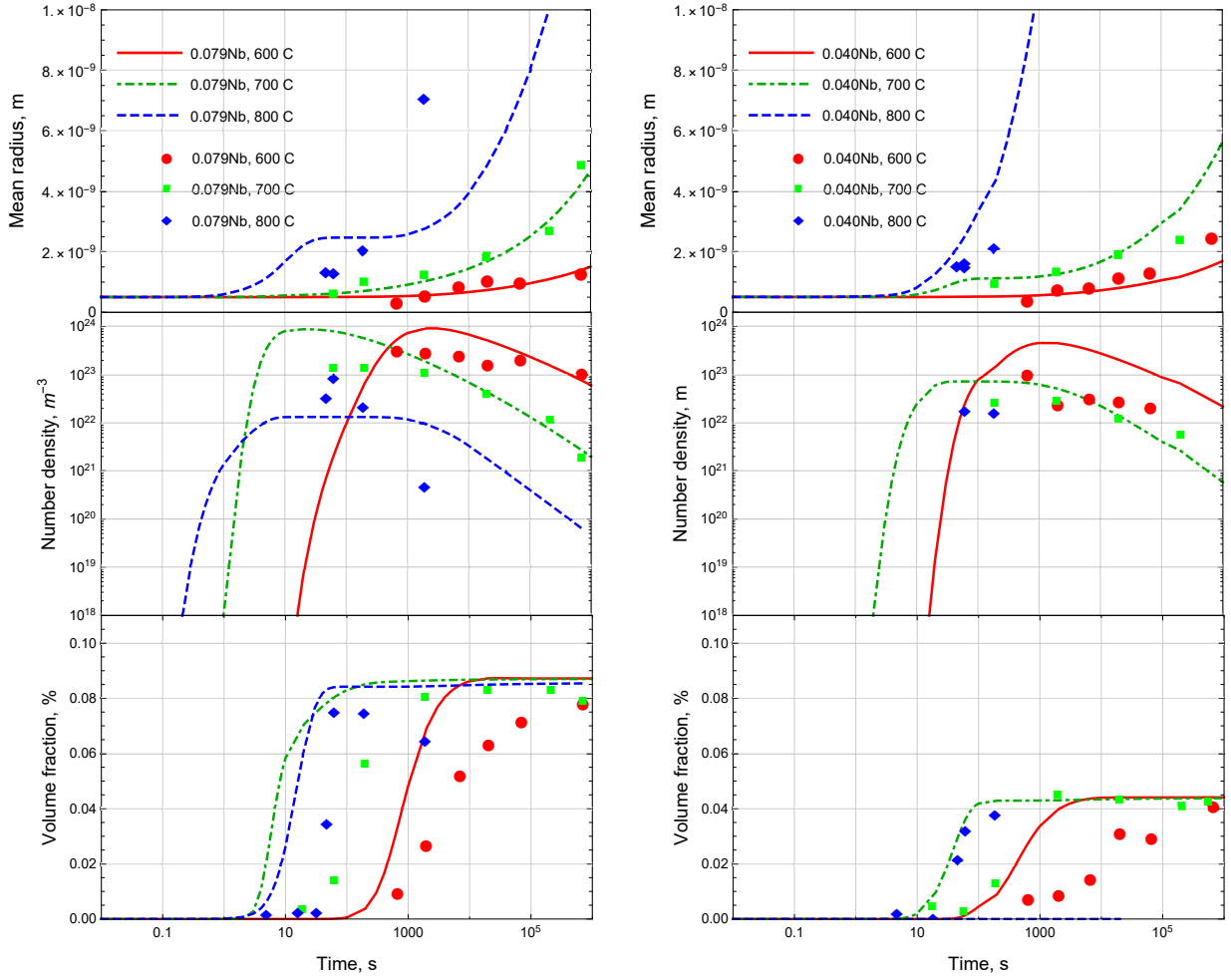


Figure 5: Simulation results for  $C(\text{wt}\% \text{Nb})=0.079$  (left) and  $0.040$  (right). The dots represent experimental data of [35, 17]. For  $C(\text{wt}\% \text{Nb})=0.040$  at  $T=800^\circ \text{C}$  the simulated number density and volume fraction of precipitates is too small and, therefore invisible in the figures.

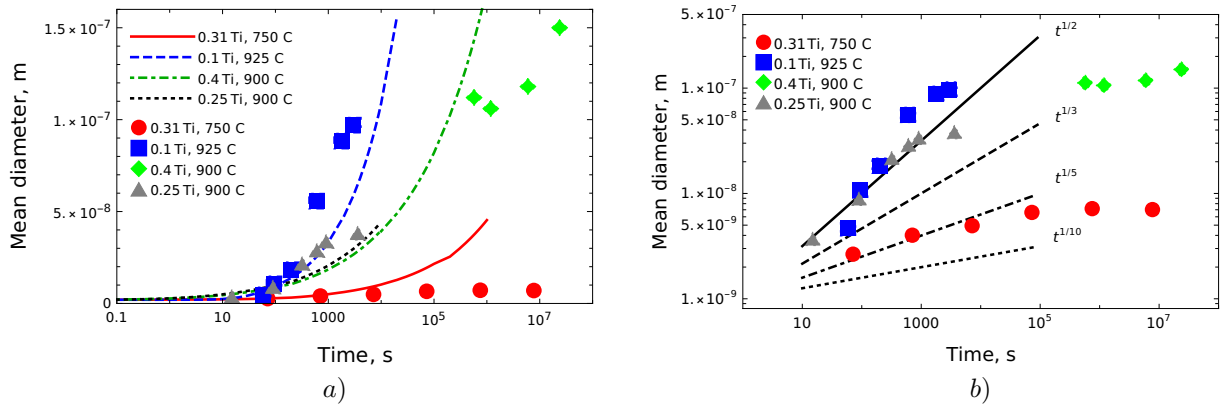


Figure 6: Comparison of simulation results with experimental data for TiC precipitates in austenitic stainless steel. The dots represent the experimental data of [25, 28, 33, 36].

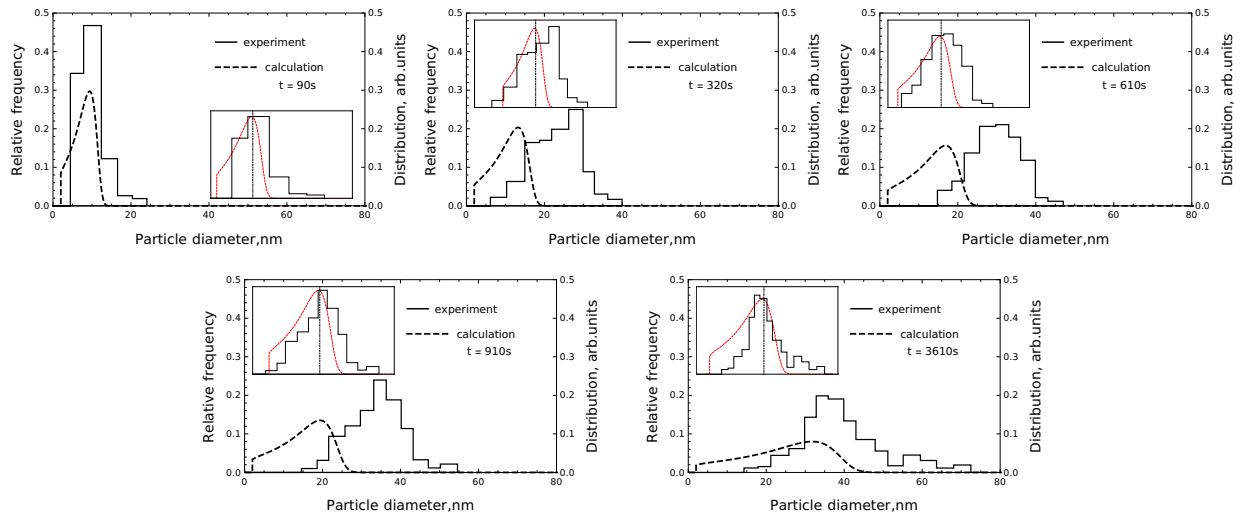


Figure 7: Size distributions from experiment [36] and simulation for different times at  $900^{\circ}\text{C}$ . The inserts inside the graphs display the experimental and calculated distributions shifted such that both have the same mean particle diameter. The dot-dashed vertical line represents mean diameter.

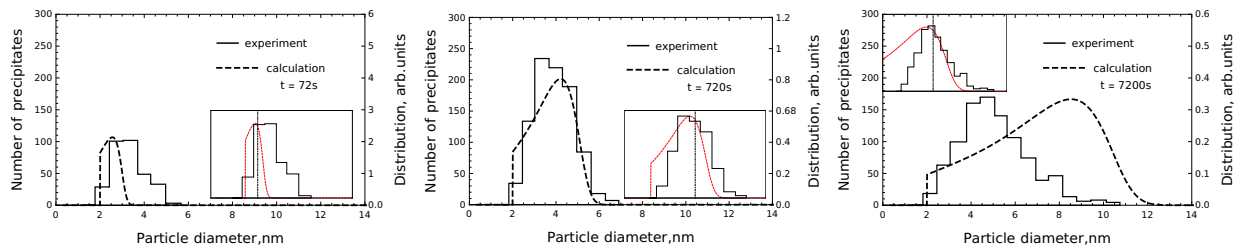


Figure 8: Size distributions from experiment [25] and simulation for different times at  $750^{\circ}\text{C}$ . The inserts inside the graphs display the experimental and calculated distributions shifted such that both have the same mean particle diameter. The dot-dashed vertical line represents mean diameter.

## References

- [1] T. Thorvaldsson and G. L. Dunlop. Precipitation reactions in Ti-stabilized austenitic stainless steel. *Metal Science*, November:513–518, 1980.
- [2] Thomas Sourmail. *Simultaneous Precipitation Reactions in Creep-Resistant Austenitic Stainless Steels*. PhD thesis, University of Cambridge, 2002.
- [3] Hao Jie Kong and Chain Tsuan Liu. A review on nano-scale precipitation in steels. *Technologies*, 6, 2018.
- [4] K. Herschbach, W. Schneider, and K. Ehrlich. Effects of minor alloying elements upon swelling and in-pile creep in model plain Fe-15Cr-15Ni stainless steels and in commercial DIN 1.4970 alloys. *Journal of Nuclear Materials*, 203:233–248, 1993.
- [5] W. Kesternich and J. Rothaut. Reduction of helium embrittlement in stainless steel by finely dispersed TiC precipitates. *Journal of Nuclear Materials*, 103-104:845–852, 1981.
- [6] W. Kesternich. A possible solution of the problem of helium embrittlement. *Journal of Nuclear Materials*, 127:153–160, 1985.
- [7] W. Kesternich and D. Meertens. Microstructural evolution of a titanium-stabilized 15Cr-15Ni steel. *Acta Metallurgica*, 34(6):1071–1082, 1986.
- [8] Takayoshi Kimoto and Haruki Shiraishi. Dose dependence of void swelling and precipitation behavior in MC carbide dispersed austenitic Fe-Ni-Cr alloys. *Journal of Nuclear Materials*, 141-143:754–757, 1986.
- [9] Niels Cautaearts, Remi Delville, Wolfgang Dietz, and Marc Verwerft. Thermal creep properties of Ti-stabilized DIN 1.4970 (15-15Ti) austenitic stainless steel pressurized cladding tubes. *Journal of Nuclear Materials*, 493:154–167, 2017.
- [10] N. Cautaearts, R. Delville, E. Stergar, D. Schryvers, and M. Verwerft. Tailoring the TiC nanoprecipitate population and microstructure of titanium stabilized austenitic steels. *Journal of Nuclear Materials*, 507:177–187, 2018.
- [11] J. Séran and M. Le Flem. *Structural Materials for Generation IV Nuclear Reactors*, chapter Irradiation-resistant austenitic steels as core materials for Generation IV nuclear reactors, page 285. Number 106 in Woodhead Publishing Series in Energy. Elsevier, 2016.
- [12] F. Christien and A. Barbu. Modelling of copper precipitation in iron during thermal aging and



- irradiation. *Journal of Nuclear Materials*, 324:90–96, 2004.
- [13] Emmanuel Clouet, Alain Barbu, Ludovic Laé, and Georges Martin. Precipitation kinetics of  $Al_3Zr$  and  $Al_3Sc$  in aluminum alloys modeled with cluster dynamics. *Acta Materialia*, 53:2313–2325, 2005.
- [14] Jia-Hong Ke, Huibin Ke, G. Robert Odette, and Dane Morgan. Cluster dynamics modeling of Mn-Ni-Si precipitates in ferritic-martensitic steel under irradiation. *Journal of Nuclear Materials*, 498:83–88, 2018.
- [15] Zhenqiang Wang, Qilong Yong, Xinjun Sun, Zhigang Yang, Zhaodong Li, Chi Zhang, and Yuqing Weng. An Analytical Model for the Kinetics of Strain-induced Precipitation in Titanium Micro-alloyed Steels. *ISIJ International*, 52:1661–1669, 2012.
- [16] B. Dutta, E. J. Palmiere, and C. M. Sellars. Modelling the kinetics of strain induced precipitation in Nb microalloyed steels. *Acta materialia*, 49:785–794, 2001.
- [17] F. Perrard, Alexis Deschamps, and Philippe Maugis. Modelling the precipitation of nbc on dislocations in  $\alpha$ -Fe. *Acta Materialia*, 55(4):1255–1266, 2007.
- [18] M.H. Mathon, A. Barbu, F. Dunstetter, F. Maury, N. Lorenzelli, and C.H. de Novion. Experimental study and modelling of copper precipitation under electron irradiation in dilute fecu binary alloys. *Journal of Nuclear Materials*, 245:224–237, 1997.
- [19] N.M. Ghoniem and S. Sharafat. A numerical solution to Fokker-Planck equation describing the evolution of the interstitial loop microstructure during irradiation. *Journal of Nuclear Materials*, 92:121–135, 1980.
- [20] M.F. Wehner and W.G. Wolfer. Vacancy cluster evolution in metals under irradiation. *Philosophical Magazine A*, 52:189–205, 1985.
- [21] Karsten Ahnert and Mario Mulansky. Odeint – solving ordinary differential equations in C++. *AIP Conference Proceeding*, 1389:1586, 2011.
- [22] Zhenqiang Wang, Qilong Yong, Xinjun Sun, Zhigang Yang, Zhaodong Li, Chi Zhang, , and Yuqing Weng. An analytical model for the kinetics of strain-induced precipitation in titanium micro-alloyed steels. *ISIJ International*, 52(9):1661–1669, 2012.
- [23] <https://www.matcalc.at/wiki/doku.php?id=techpapers:precipitation:diffusion>.
- [24] S. S. Hansen, J. B. Vander Sande, and Morris Cohen. Niobium carbonitride precipitation and austenite recrystallization in hot-rolled microalloyed steels. *Metallurgical Transactions A*, 11A:387–402, 1980.
- [25] W. Kesternich. Dislocation-controlled precipitation of TiC particles and their resistance to coarsening. *Philosophical Magazine A*, 52(4):533–548, 1985.
- [26] Jae Hoon Jang, Chang-Hoon Lee, Yoon-Uk Heo, and Dong-Woo Suh. Stability of (Ti,M)C (M = Nb, V, Mo and W) carbide in steels using first-principles calculations. *Acta Materialia*, 60:208–217, 2012.
- [27] Sheldon H. Moll and R. E. Ogilvie. Solubility and diffusion of titanium in iron. *Transactions of the American Institute of Mining and Metallurgical Engineers*, 215:613–618, 1959.
- [28] Asa Gustafson. Coarsening of TiC in austenitic stainless steel — experiments and simulations in comparison. *Materials Science and Engineering: A*, 287(1):52 – 58, 2000.
- [29] Luca F. S. Dumitrescu and Mats Hillert. Reassessment of the solubility of tic and tin in fe. *ISIJ International*, 39(1):84–90, 1999.
- [30] Heilong Zou and J.s. Kirkaldy. Carbonitride precipitate growth in titanium/niobium microalloyed steels. *Metallurgical Transactions A*, 22A:1511–1524, 1991.
- [31] S. Kurokawa, J. E. Ruzzante, A. M. Hey, and F. Dymont. Diffusion of Nb in Fe and Fe alloys. *Metal Science*, 17:433, 1983.
- [32] Q.L. Yong, Y.F. Li, and Z.B. Sun. Theoretical calculation of specific interfacial energy of semicoherent interface between microalloy carbonitrides and austenite. *Acta Metallurgica Sinica*, 2:153–156, 1989.
- [33] Zhenqiang Wang, Xinjun Sun, Zhigang Yang, Qilong Yong, Chi Zhang, Zhaodong Li and Yuqing Weng. Carbide precipitation in austenite of a Ti–Mo-containing low-carbon steel during stress relaxation. *Materials Science and Engineering A*, 573:84–91, 2013.
- [34] Zhenqiang Wang, Han Zhang, Chunhuan Guo, Zhe Leng, Zhigang Yang, Xinjun Sun, Chunfa Yao, Zhengyan Zhang, and Fengchun Jiang. Evolution of (Ti, Mo)c particles in austenite of a Ti–Mo-bearing steel. *Materials and Design*, 109:361–366, 2016.
- [35] F. Perrard, A. Deschamps, F. Bley, P. Donnadieu, and P. Maugisb. A small-angle neutron scattering study of fine-scale NbC precipitation kinetics in the  $\alpha$ -Fe–Nb–C system. *Journal of Applied Crystallography*, 39:473–482, 2006.
- [36] W.J.Liu and J.J. Jonas. Ti(CN) Precipitation in Microalloyed Austenite during Stress Relaxation. *Metallurgical Transactions A*, 19A:1415–1424, 1988.